Engineering and Technology Journal
Journal homepage: https://etj.uotechnology.edu.iq

Innovative self-healing concrete using polycarboxylate ether: a fused deposition modeling approach with 3D-printed polylactic acid vascular networks

Noor A. Hameed *, **Alaa A. Abdul-Hamead, Farhad M. Othman**

Materials Engineering Dept., University of Technology-Iraq, Alsina'a street, 10066 Baghdad, Iraq.
*Corresponding author Email: Mae.20.101@grad.uotechnology.edu.iq

HIGHLIGHTS

- The 3D vascular to release healing materials at a specified crack
- A pre-and post-healing study examined the microstructure of interior fissures
- EDX analysis confirmed the consumption of $Ca(OH)_2$ and the generation of C-S-H
- Mechanical properties and durability were restored within 28 days after damage

ARTICLE INFO

Handling editor: Wasan I. Khalil

Keywords:

Polycarboxylate ether; Self-healing concrete; Nano fly ash powder; Vascular tubes.

ABSTRACT

Concrete's fracture susceptibility is due to its limited tensile strength, which can lead to cracks. Steel reinforcement is added to designated areas to address this issue, but minuscule cracks can allow liquids and vapors to infiltrate the reinforcing material, causing corrosion. Self-healing concrete can resist corrosion by mending and sealing minor cracks. This study aims to determine if fused deposition modeling (FDM) can fabricate innovative vascular networks and tubes from polylactic acid (PLA) created by using three-dimensional (3D) printing methods, and its characteristics were contrasted with those of two- and one-dimensional (2D) networks.The dimensions of the internal and exterior diameters were 4 and 5.6 mm, respectively. The researchers used a planetary ball mill to apply an organic polycarboxylate ether liquid and fly ash nanopowder to all vascular architectures. The prefabricated tubes were then incorporated into a concrete beam to enable self-repairing capabilities. The water-to-cement ratio was 0.6%; the mixture was 1 part cement, 2.16 parts water, and 2.98 other ingredients. The self-healing properties were assessed using a four-point bending test. The developed pipes can produce self-healing concrete by introducing nano fly ash particles and low-viscosity healing solutions into the blood vessel network, enabling the concrete to undergo self-repair mechanisms. The specimen that had 3D treatment restored its strength to 95% at flexural recovery.

1. Introduction

Concrete is often regarded as the predominant construction material because of its excellent compressive strength and advantageous economics. Concrete has a significantly reduced tensile strength [1,2]. Concrete's brittleness makes cracking inevitable, making it susceptible to aggressive chemicals. Its durability is influenced by its structural and micro- and macro-structural properties[3,4]. Most cracks result from limited tensile strength, creep, earthquakes, permeability, heat stress, excess load, etc. [5]. The self-healing mechanism is a helpful substitute for traditional concrete component rehabilitation and damaged repair methods [6-8], executed by using a variety of techniques either autonomously (Bacteria, capsule) or autogenously (fiber, supplementary cementitious material (SCM)). Nonetheless, the autogenous repair is limited by the fracture width. The crack has to be 200 µm or smaller [9]. One real-world instance of autonomous healing involves the little release of a therapeutic substance in polymer, glass, ceramic, and ZnO capsules [10-13].

Limited healing agents are provided via capsule-based self-healing, which reduces the requirement for bigger crack restoration and repeated damage repair [13]. A major benefit of the vascular systems is that they allow for repeated cycles of breaking and healing since the flow networks provide a constant supply of the healing agent [13]. Research looks at how the vascular system affects the healing of cracks in cementitious materials and how recycled resources are used to make concrete.

This research looked at the flexural properties of self-healing concrete railway sleepers (SHCRS) after installing polyurethane (PU)-reinforced glass tubes. Shaikh Mohammad Kouhi and others reported an observed increase of 11% in the applied stress [14]. T. Selvarajoo et al. devised a technique for delivering cyanoacrylate and evaluated its efficacy on notched prisms without reinforcement by incorporating PET tube networks into cementitious matrices [15]. Wan et al. produced wax-

http://doi.org/10.30684/etj.2024.145499.1655
Received 23 December 2023; Received in revised form 16 January 2024; Accepted 03 March 2024; Available online 26 March 2024
2412-0758/University of Technology-Iraq, Baghdad, Iraq

coated vascular networks using soluble polyvinyl alcohol filament, which were then integrated with cementitious mortar. Experiments were carried out to determine the effectiveness of epoxy resin as a healing agent [16]. A three-dimensional PLA vascular network that is biomimetic was designed and fabricated using the equation for the Murray circulatory blood volume transfer. The material was broken up. Then, sodium silicate was pumped into it for four weeks. The sample's mechanical characteristics were then evaluated using the load recovery method developed by Li et al. [17]. Using 3D printing technology, Eleni Tsangouri et al. created therapeutic polymer tubes that broke when fractured, enabling the application of polyurethane healing foam and strengthening and resilient tissue to be restored [18].

This work created a composite material to fill up fractures up to 400 μm deep by combining cement with superabsorbent polymers. A concrete self-healing capsule containing cement or a combination of cement and polyethylene glycol was developed, demonstrating improved sealing ratios, water tightness, flexural strength, and compressive strength [19]. An investigation was conducted to examine how self-curing chemicals affected concrete's durability. The M30 concrete mixture was supplemented in the experiment using Sodium Polyacrylate, Polyethylene glycol (PEG), propylene Glycol (PPG), Perlite, and Vermiculite. The results showed that PEG and PPG were the most effective self-curing substances [201]. Through the process of encapsulating sodium alginate inside polyethylene glycol granules that are then coated with epoxy resin and calcium sulfoaluminate cement, Jianhang Feng et al. were able to produce hydrogels effectively. Within twenty-four hours [21], Azam Torkan and colleagues created a new method for smart cracking of cementitious structures using fibrous media containing polyethylene glycol and silicon dioxide nanoparticles. This method hydrates and heals cracks, demonstrating increased healing efficiency due to a decreased fracture radius, as demonstrated by FESEM, EDS analysis, and ultrasonic testing [22]. Wu et al. The study explores using fibers and capsules in cement mortar to delay crack occurrence and enhance self-healing capacity, revealing that adding OH-rich polyvinyl alcohol and sisal fibers enhances mortar mechanical properties [23].

Several factors affect the effectiveness of adsorption and preserving slump, including the main and side chains of various types, including the stabilization group, and the molecular weight of carboxylate-type plasticizers in concrete mixtures used as superplasticizers to reduce water content. It has been shown that longer chains enhance adsorption capacities by Sha et al. [24].

The study explores the impact of polycarboxylate ether-based superplasticizer (PES) on the mechanical strength of cemented paste backfill. It aims to create a 3-D vascular tube to improve the distribution and coverage of healing agents. Comparable one-dimensional and two-dimensional networks were used to assess the vascular network's potential for concrete self-healing. The research found that the polylactic acid structures have a mechanically activated interfacial connection and a brittle fracture reaction. The widths of the first fractures seen in each system ranged from 600 to 800 μm. The experiment results showed that the pumped polycarboxylate ether liquid could be transported through the vascular network of all three systems for seven to twenty-eight days, including powdered nano fly ash as a healing agent. The self-healing effect's mechanism was explained in terms of the load-bearing capacity recovered during the mechanical assessment after the specimen underwent four-point bending and force was applied again. A wider spectrum of medicinal compounds may be investigated by this research, and it will also help to enhance cement compositions, which is crucial for advancing concrete technology and building techniques.

2. Experimental Study

The experimental study comprises four distinct components:

2.1 Vascular tube and network fabrication using 3D printing technology

The vascular tubes and networks were created using additive manufacturing methods, including 3D printing, with geometric configurations, including one-, two-, and three-dimensional (3D) designs. The 0.80 mm nozzle-equipped Creality CR-10S 3D printer created the vascular. The printer can print up to 300 mm by 300 mm by 400 mm at a maximum size, 60 μm at a maximum print resolution, and 80 mm/s at a maximum print velocity. The two main biodegradable polylactic acid (PLA) sources are corn and sugarcane. The glass transition temperature (Tg) of polylactic acid (PLA) is comparatively low at 60 ℃, and its elongation at break is just 10% [25]. The tubes under consideration possess a volumetric capacity of 30 ml with a length of 100 mm. The internal diameter of these tubes is 4 mm, while the exterior diameter measures 5.6 mm. The filament printing parameters used to produce Fused Deposition Modeling (FDM) samples are shown in Table 1.

The efficiency of self-healing tubes greatly depends on their ability to maintain the PLA's chemical stability in a cementitious matrix, conserve the healing agent, and prevent agent leaking before a pipe breaks. The interlayer adhesion of Fused Deposition Modeling (FDM) pipes is strong. The pipes and the concrete don't seem to be spaced apart.

Tubes were constructed utilizing each unique filament and then filled with an appropriate substance to assess the mechanical recovery of plastic filaments after breakage and subsequent embedding into a cube of concrete during the casting process. A magnetic stirrer combined the nanopowder with a polycarboxylate ether (SP) solution. The mixture was injected into the tubes using a syringe as a healing agent. The specimens were submerged in water for 28 days before being divided to examine the efficacy of the therapeutic substances. The liquid state of the healing component suggests that the use of Polycarboxylate ether might potentially facilitate the process of self-healing.The efficiency of self-healing tubes greatly depends on their ability to maintain the PLA's chemical stability in a cementitious matrix, conserve the healing agent, and prevent agent leaking before a pipe breaks. The interlayer adhesion of Fused Deposition Modeling (FDM) pipes is strong. The pipes and the concrete don't seem to be spaced apart.

Tubes were constructed utilizing each unique filament and then filled with an appropriate substance to assess the mechanical recovery of plastic filaments after breakage and subsequent embedding into a cube of concrete during the casting process. A magnetic stirrer combined the nanopowder with a polycarboxylate ether (SP) solution. The mixture was injected into the tubes using a syringe as a healing agent. The specimens were submerged in water for 28 days before being divided to

examine the efficacy of the therapeutic substances. The liquid state of the healing component suggests that the use of Polycarboxylate ether might potentially facilitate the process of self-healing.

Table 1: Displays the various configurations of printing settings specifically designed for PLA material

The parameters associated with the process of printing	The configurations
Height of the layer (mm)	0.1, 0.2, 0.3, 0.4, 0.5
The orientation of layers	Upright
Temperature printing (℃)	215
The temperature of the bed (℃)	60
The filament's diameter (mm)	1.75
The nozzle's diameter (mm)	0.8
The printing speed (mm/s)	50 mm/s
angle of raster	45/-45
Speed of travel (mm/s)	150 mm/s
Infill	100%

2.2 Activation fly ash

The manufacture of Nanopowder from fly ash was conducted using a planetary ball mill equipped with porcelain balls, operating at a rotational speed of 400 revolutions per minute (rpm) for three hours.

2.3 Materials used

2.3.1 Cement

Type (I) ordinary Portland cement was used in the present investigation. Additionally, the cement satisfies the standards of the ASTM (C150-04) and the Iraqi Specification (No. 5/1984) [26] in terms of both its physical and chemical composition [27], and the chemical composition of cement is shown in Table 2.

Table 2: Used cement chemical composition and physical properties

Chemical components %	Fe_2O_3	SO_3	SiO_2	$Al2O_3$	CaO	MgO	Alkalies (K2O, Na2O3)	LOI	C3A	C3S	C2S	C4AF	LSF
Cement	3.13	2.06	20.07	5.74	62.29	2.32	0.60	1.91	9.92	58	13.80	9.52	0.96
Physical properties													
		The initial setting, min					52	Min.45					
		The final setting, hr					5	Max.10					
		Compressive strength at 28 days, MPa					27	23					

2.3.2 Aggregate

Coarse aggregates with a grade maximum of 20 mm are currently in stock. The fine aggregates consist of natural sand with a particle size of 4.75 mm, sourced from the Mustafa plant in Karbala. The materials adhere to the standards set by ASTM (C33-03) [28] as well as the Iraqi Standardization (No. 45/1984) [29]. The sieving machine used is shown in Table 3 as compatible with zone 3, and physical properties are shown in Table 4.

Table 3: Classification and specifications for fine aggregate grading

Size of sieve (mm)	Cumulative pass rate (%)	Cumulative passing (%) in accordance with IOS No. 45/1984's limitations
4.750	100.0	90-100
2.360	92.220	85 - 100
1.180	85.370	75 - 100
0.600	68.250	60 - 79
0.300	27.530	12 - 40
0.150	9.110	0 -10

Table 4: The physical properties of sand

Features	Specifications	Results	Specifications for Iraq No. 45/1984
Particular Gravity	2.640	2.640	-
Absorption percentage (%)	0.770	0.770	-
Weight of a dry loose unit (kg/m^3)	1591	1591	-
The percentage of sulfate content as SO_3	0.090	0.090	≥ 0.50
The percentage of material that is smaller than the 75 µm sieve.	3.90	3.90	≥ 5

2.3.3 Fly ash

A byproduct of coal combustion is a fine powder of inorganic materials carried away with flue gases during the combustion. The class F fly ash used in the study met the specifications outlined within the ASTM American Standard (C 618-15), as shown in Table 5 [30].

Table 5: Used fly ash chemical composition and physical properties

Chemical components %	Fe_2O_3	SO_3	SiO_2	Al_2O_3	CaO	MgO	Na_2O	L.O.I
Fly ash	**2.67**	**4.3**	**55.87**	**20.82**	**8**	**0.34**	**0.26**	**5.6**
Physical Properties								
Physical appearance				Powders				
The color				Gray				
Specific weight				2				
Strength Activity Index with Portland				96.89				

2.3.4 polycarboxylate ether

The chemical additive utilized in this study as a healing agent is called superplasticizer (SP). Specifically, the superplasticizer used in this study is Sika Visco Crete-5930 L, which Sika supplies for construction chemicals/in Iraq. It is worth noting that this product is in accordance with the BS EN 934-2:2001 standard [31]. Table 6 presents the properties of SP.

Table 6: Superplasticizer (Sika ViscoCrete-5930) characteristics

Form	Viscous liquid
Basis	Aqueous solution of modified polycarboxylate
Appearance	Turbid liquid
Density	1.1 $kg/1L$

2.4 Mixture proportions

The frequently used weight ratio (1:2 , 16:2.98) was used for mixing to attain 30 MPa in 28 days. Each cubic meter of the composite contains 340 kilograms of cement, 734.4 kilos of sand, and 1013.2 kilograms of gravel. The ratio of water to cement is 0.6 . This study was prepared according to British Standard BS 5328-2:1997. The research created an autonomous self-healing system by adding 10% Ultrafine fly ash powder to hollow tube healing fluid, which is shown by incorporating a concrete mixture as outlined in Table 7. The development of an autonomous self-healing system is proposed and described in Table 8.

Table 7: Mixture of the concrete beam proportions compressive and flexural strength specimens

Mix	Nano fly ash (g)	Polycarboxylate ether liquid (ml)	Cement (g)	Fine aggregate (g)	Coarse aggregate (g)	Water (ml)	Sample number
Control cube	0	0	1148.56	2480.8	3422.7	689.1	6
Cube with vascular tube	1	5	1148.56	2480.8	3422.7	689.1	18
Control prism	0	0	1701	3674	5069	1020	6
Prism with vascular network	4	20	1701	3674	5069	1020	18

The present research prepared cubes and prisms to test hardened concrete's mechanical capabilities. After 7 and 28 days and the addition of fractured samples, cured concrete specimens were air-conditioned for 28 days to heal. After that, the specimen's compressive strength was tested. BS (1881-116) [32] defined three tests for 150 x 150 x 150 mm cubic specimens. 500 x 100 x 100 mm Three beams were made to test concrete samples' flexural strength at 7 and 28 days using a four-point flexural machine, per ASTM (C78) [33]. A unique circulatory system was incorporated using one-, two-, and three-dimensional designs. Metal bars with a smooth surface measuring 4 millimeters in diameter were used to avoid total splitting during cracking and were placed 10 mm from the bottom of the specimens. The specimens were forced until the beams on two supports, 400 mm apart, at both ends failed. The results showed the fresh properties of the concrete beam, where the value of slump was 4 cm, and the fresh density was 2271 kg/m^3.

Table 8: Description of the healing system used in concrete beam

Healing system	Outer diameter	Input diameter	Length	Volume	Healing material
Vascular tube for cube	5.6 mm	4 mm	100 mm	5 ml for 1D,2D,3D	Mix (polycarboxylate+10% nano fly ash)
Vascular network for prism	5.6 mm	4 mm	400 mm	20 ml for 1D,2D,3D	Mix (polycarboxylate+10% nano fly ash)

3. The process of inspections and testing

3.1 Examination of nanopowders

This device is a Brookhaven Nano Brook 90 Plus model manufactured in the United States and was used at the Center of Nanotechnology and Advanced Research to analyze the particle size of fly ash powder. The findings showed that the particles had a size of 100 nanometers.

3.2 Test of compressive strength

One method for determining a material's ability to withstand compressive forces is the test for measuring compressive strength. The protocol for this test was followed, as stated in BS (1881-116) [34]. The following formula is used to determine compressive strength:

$$\sigma = \frac{P}{A} \quad (1)$$

The compressive strength, denoted by the symbol σ in the equation 1, is expressed in megapascals (MPa). The variable denotes the specimen's cross-sectional area, expressed in square millimeters (mm^2), and the maximal compressive force, expressed in Newtons (N). With the main goal of analyzing the compressive strength, the arrangement of the tubes and how they distribute the healing material within the cubic construction are shown in Figure 1.

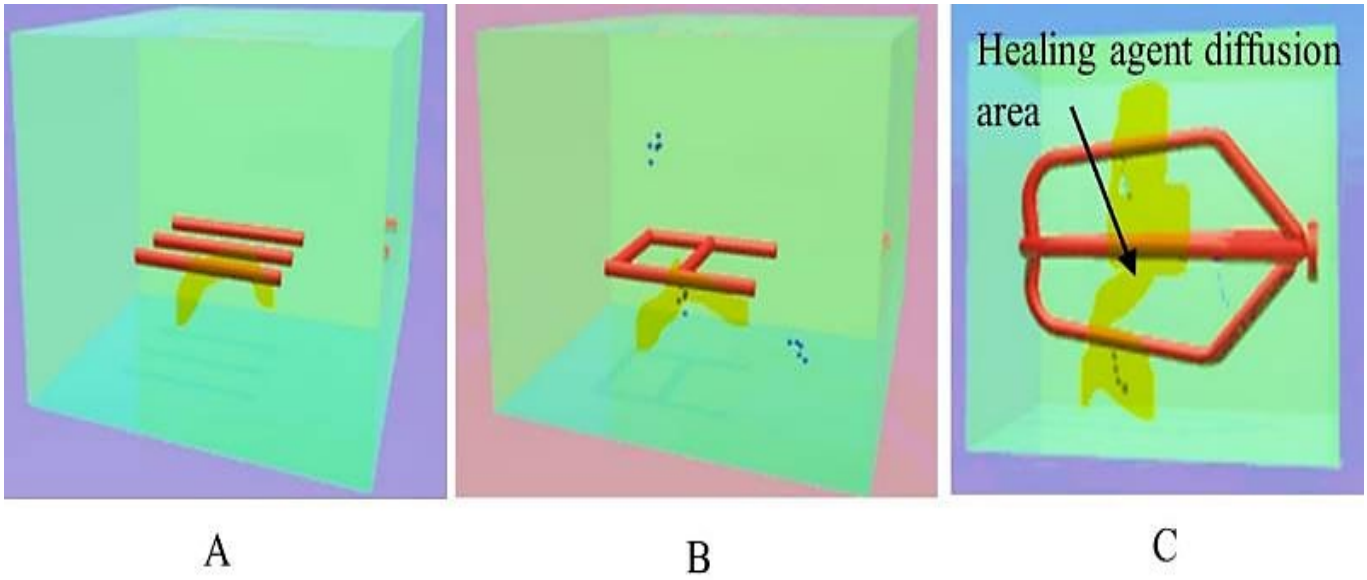

Figure 1: Shows a specimen with a vascular tube with different design in cube (a) a one, (b) two, and (c) three-dimensional

3.3 Recovering flexural strength test

The ASTM (C78) [35] guidelines were followed to evaluate the bending strength. A 3 mm notch was made before the four-point bending test was performed. A measurement of 0.2 MPa/s was made for the download rate. After the test, the samples underwent an air-drying procedure and were left undisturbed for four weeks. Equation 2 may be used to calculate the specimens' bending strength for the two initial (1st R) and the subsequent iteration (2nd R).

$$Fct = \frac{F*I}{d1*d2^2} \quad (2)$$

Here, the flexional force (Fct) is expressed in Newtons per square millimeter (N/mm^2) or megapascals (MPa). Newton (N) measures the ultimate load (F). The distance between the two supporting rollers in millimeters (mm) is shown by the span (I). Moreover, the lateral dimensions of the specimen, which are also expressed in millimeters (mm), are reflected in (d1) and (d2). In addition, after four weeks of healing, the prism specimens with similar properties in both groups performed an additional examination, referred to as the second R. To evaluate the recovery of flexural strength throughout this assessment, pertinent equations were used, as described in reference [36].

$$\eta\% = \frac{Fct2}{Fct1} \quad (3)$$

The highest level of stress that the original specimen encountered during the initial rupture (with the first "R") is represented by fct1, the maximum stress that the specimen attained after healing (second R) is represented by fct2, and the efficacy of the healing process is shown by $\eta\%$. A fissure-detecting microscope was used to examine the fracture barrier many times. The depth and width of the fracture were measured using photographic evidence to calculate the percentage of strength

that the crack could restore over a certain time. It was possible to determine where the measurements were taken and if any broken prisms were present. The configuration of the blood vessels within the prism is shown in Figure 2.

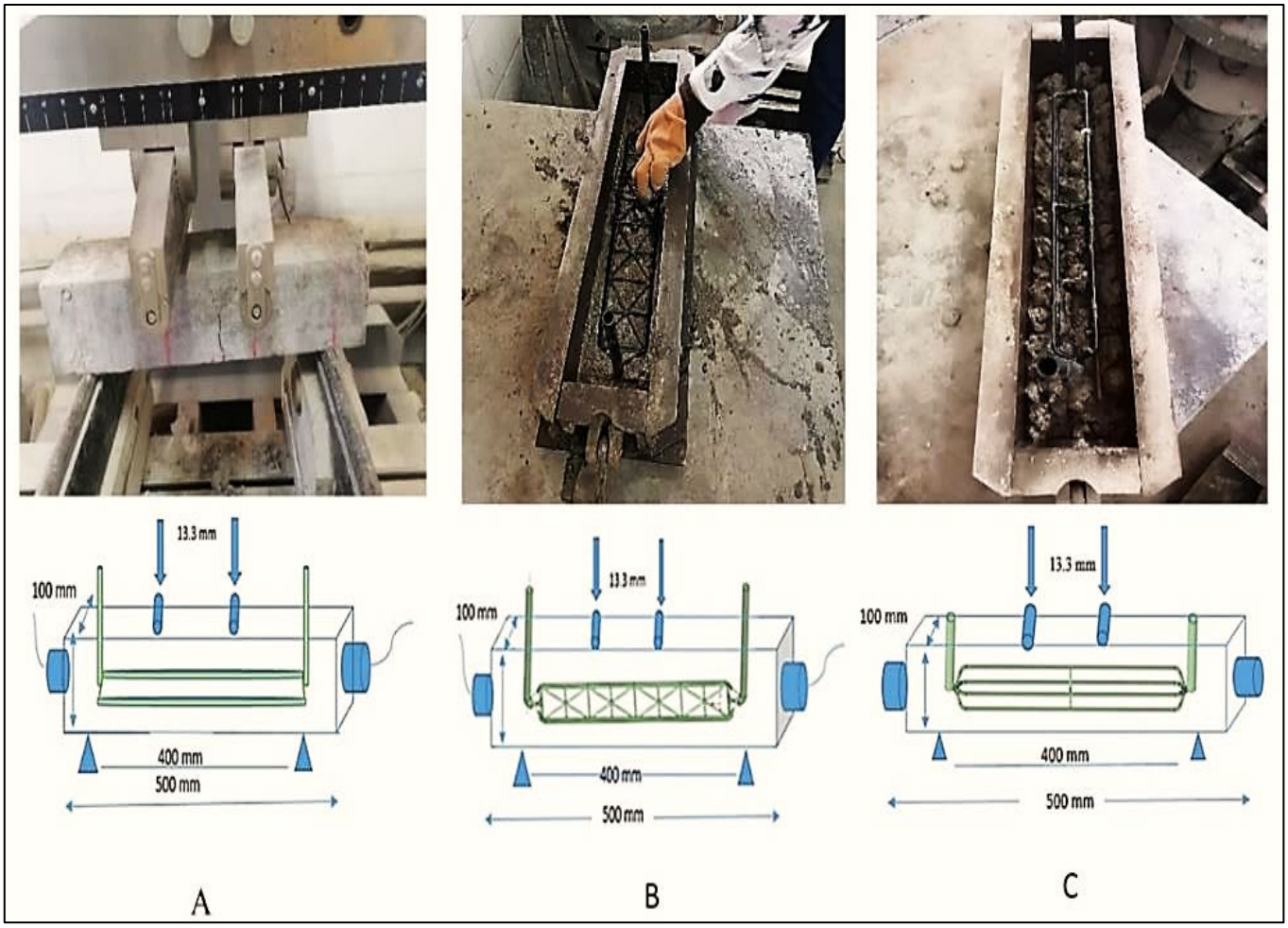

Figure 2: Displays a prism specimen with embedded a vascular tube that has been placed in three different dimensions(a) 1D, (b) 2D, and (c) 3D

3.4 Field emission scanning electron microscopy (FESEM) and energy-dispersive X-ray spectroscopy (EDS)

Utilizing a blend of cutting-edge imaging methods from Nanoazma Lab in Tehran, Iran, like EDS, VP FE-SEM, Sigma, Zeiss, etc, we examined the morphology of the surface of specimens that had healed and those that hadn't. We used a FESEM at different magnifications to examine the specimens, from 100 µm to 10 m. Furthermore, we determined the elemental composition using EDS.

3.5 FTIR (Fourier transform infrared) spectrum tests

This approach is used to get a comprehensive understanding of the atomic organization and chemical bonding formation in materials made of polymers. The test followed the ASTM E1252 guidelines, using a Brukeroptier TENSOR-27 Fourier infrared (FI) spectrometer at Nanoazma Lab in Tehran. The 400-4000 cm^{-1} range was used for the infrared spectrum [37].

4. Results and discussion

4.1 Particle size analysis (PSA)

The fly ash nanoparticles generated by the planetary ball milling technique were assessed using a particle size analyzer (PSA) to determine the size and dispersion of the particles after the milling process. According to the PSA, the fly ash particle diameter was effectively reduced to 95.3 nm throughout a three-hour milling operation. It is shown that a Nanoparticle size distribution significantly improves the healing ability. The synthesized FA nanopowder's distribution of particle sizes is shown in Figure 3.

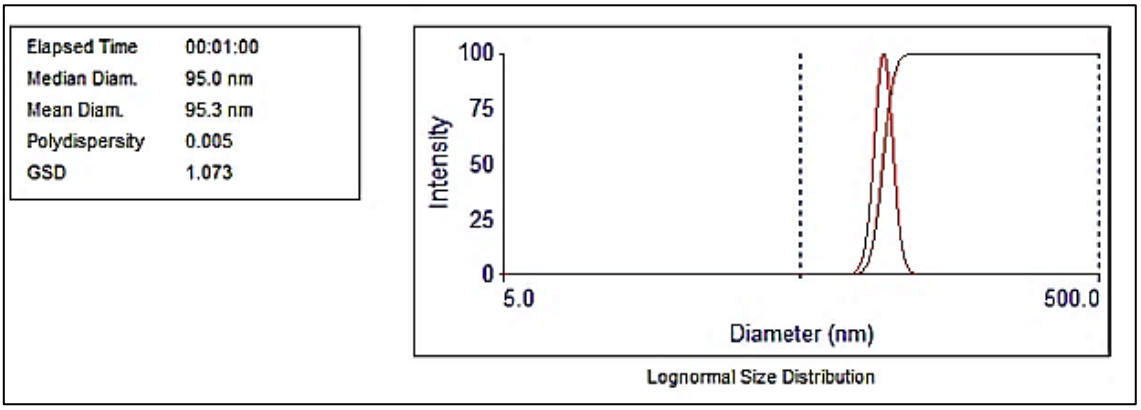

Figure 3: Particle size distribution for the prepared nano fly ash after milling

4.2 Compressive strength

The test for compressive strength results are shown in Figure 4, including cube samples taken at 7-day and 28-day intervals. The obtained outcomes show the averages of the three different samples. The significant surface area of nano-fly ash (NFA) particles may cause the observed improvement in compressive strength when NFA particles are combined with polycarboxylate ether. A large enough surface area might act as a nucleation site, encouraging the development of the C-S-H gel and other hydration products [38, 39]. Combining a chemical that facilitates healing with poly(lactic acid) (PLA) tubes made of a water-repellent substance yields a cohesive mixture. The cube is subjected to a 28-day air curing time once the healing agent is released upon the occurrence of a fracture. Moreover, the uniform distribution of sulfate particles (SP) in the concrete may have contributed to increased compressive strength by encouraging the gel phase's continual hydration. In concrete, fly ash, polycarboxylate ether superplasticizers (SP), and calcium hydroxide ($Ca(OH)_2$) interact favourably. It can close capillary pores, reduce permeability, and shrink pores. The fact that SP causes an increase in the density of C-S-H gel is supported by earlier research findings. Compressive strength was significantly increased when a medicinal ingredient was integrated with a three-dimensional (3D) design. In particular, after 7 and 28 days, compressive strength was significantly increased by 26.6% and 37%, respectively [40].

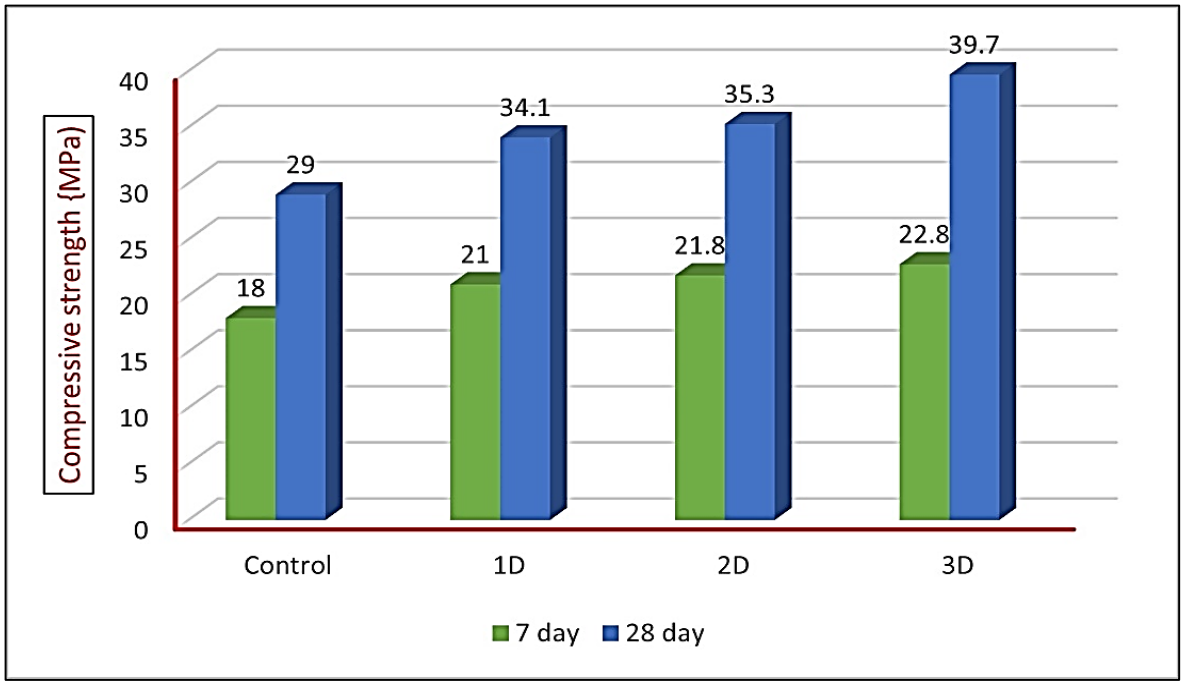

Figure 4: The results of the measurement for compressive strength

4.3 Flexural strength recovery

The restoration of load-bearing capacity after the healing treatment was used to measure the effectiveness of mechanical stimulation and circulatory system regeneration, as shown in Figure 5 (a). Four-point bending tests were used on prefabricated vascular networks in one, two, and three dimensions to induce fracture development in the samples deliberately. Figure 5 displays the test findings that were achieved. The initial load testing revealed a limited load response with recorded values of around 4.5 MPa and 5.5 MPa on plain concrete beams that underwent maturation periods of 7 and 28 days. The force needed to shatter the control specimen and the specimens implanted with vascular networks showed a clear disparity. An illustration of this discrepancy may be seen in Figure 5 (a). The polylactic acid (PLA) tubes or the physical activation may be to blame for

this behaviour. Furthermore, it has been shown that high strain may cause fractures in the vascular systems, which include the 1D, 2D, and 3D structures. The use of plastic tubing increased the cement beams' longevity.

Equation 3 was used to evaluate the flexural strength recovery. Following a 28-day healing interval, Prism samples from the two combinations were submitted for evaluation, as shown in Figure 5 (b). According to the findings, the specimen that had 3D treatment restored its strength to a level of 95%, but the control specimen only recovered at a pace of 43%. Analyzing the results regarding the control group showed that MC was an effective therapeutic drug, which is in line with other studies. Function as starting and promoting points for producing calcium-silicate-hydrate (C-S-H) compounds [41,42]. The three-dimensional structure of the vascular system shows a greater ability to block a greater region of the fracture than the one-dimensional (1D) and two-dimensional (2D) systems. The insufficiency of the systems in 1D and 2D in supplying the healing agents to this specific area was caused by the capillary force's incapacity to promote the upward migration of the healing substance and close the crack tip. Compared to the 1D design, the 2D and 3D networks exhibit a higher stress tolerance, which might be explained by the many supporting infrastructures and lack of focus on a single tube.

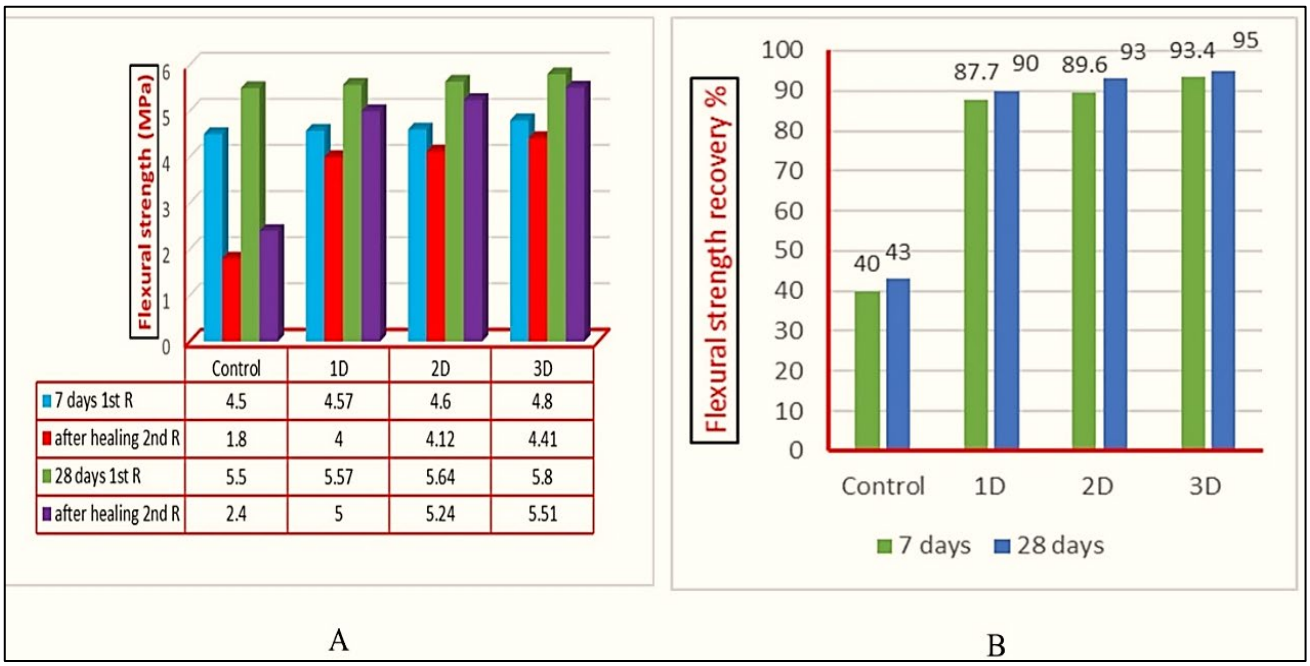

Figure 5: Concrete flexural strength with varied vascular tube designs (a) Each sample has a unique design at 1st R and 2nd R (b) Flexural strength percentage recovery of sample with differend design vascular tube.

4.4 Analysis of microstructure development

Scanning electron microscopy was used to analyze broken surfaces before and during self-repair. Figures 6 (a, b) show this. As demonstrated in Figures 6 (c, d) self-healing materials were present on cracked surfaces and had a different composition from the interior cement paste. The product layer was seen to expand outward, beginning at the crack's surface and moving into its core. The evaluation and analysis of microstructure's expansion and development. The bulk of the cracks in the experimental sample were filled with distinct CH crystals and a significant quantity of CSH gel, which resulted from unreacted cement particles serving as self-healing agents. Polycarboxylate superplasticizer enhances the microscopic structure of hydration products in cementitious materials. It decreases the size of crystals such as $Ca(OH)_2$, AFt, and other hydration products. Additionally, it speeds up the transformation of ettringite AFt into AFm. Including superplasticizer also impacts the pore structure since cement particles in newly mixed pastes tend to aggregate into flocculates owing to van der Waals force or electrostatic interactions. The superplasticizer molecules adhere to the cement grain surface, causing the disintegration of the flocculates and facilitating the improved dispersion of fly ash. The presence of nanofillers in FA triggers the pozzolanic reaction, whereby FA particles use the C-H by-product to generate C-S-H gel. Polycarboxylate improves the uniformity and roundness of sand particles, leading to more hydration of cement particles and a thicker layer of sand coating. This has the potential to enhance compressive strength. The polycarboxylate water-reducing agent (PCE) is composed of polymer backbones containing carboxyl groups, resulting in a substantial decrease in water content compared to conventional alternatives [43-45].

A comprehensive analysis of the resultant chemical compositions was made possible by the numerical data obtained from the EDX investigation. The degree of hydration of the calcium-silicate-hydrate (C-S-H) gels was measured using the atomic ratio of calcium to silicon (Ca/Si). $Ca(OH)_2$ consumption during cement hydration rose as the Ca/Si ratio dropped. As a result, C-S-H linkages were formed, and the densification of the concrete matrix was significantly aided by the nanofiller effect. Calcium hydroxide (CH) is produced in the first stages of the curing process. This causes more calcium-silicate-hydrate (C-S-H) binder gel to develop by starting the pozzolanic reaction with non-ferrous aggregates (NFA). This investigation evaluated the effect of Sp liquid, which comprises nano fly ash, on the microstructure's dimensions. Energy-dispersive X-ray spectroscopy (EDS) and scanning electron microscopy (SEM) were used in the assessment. [46,47].

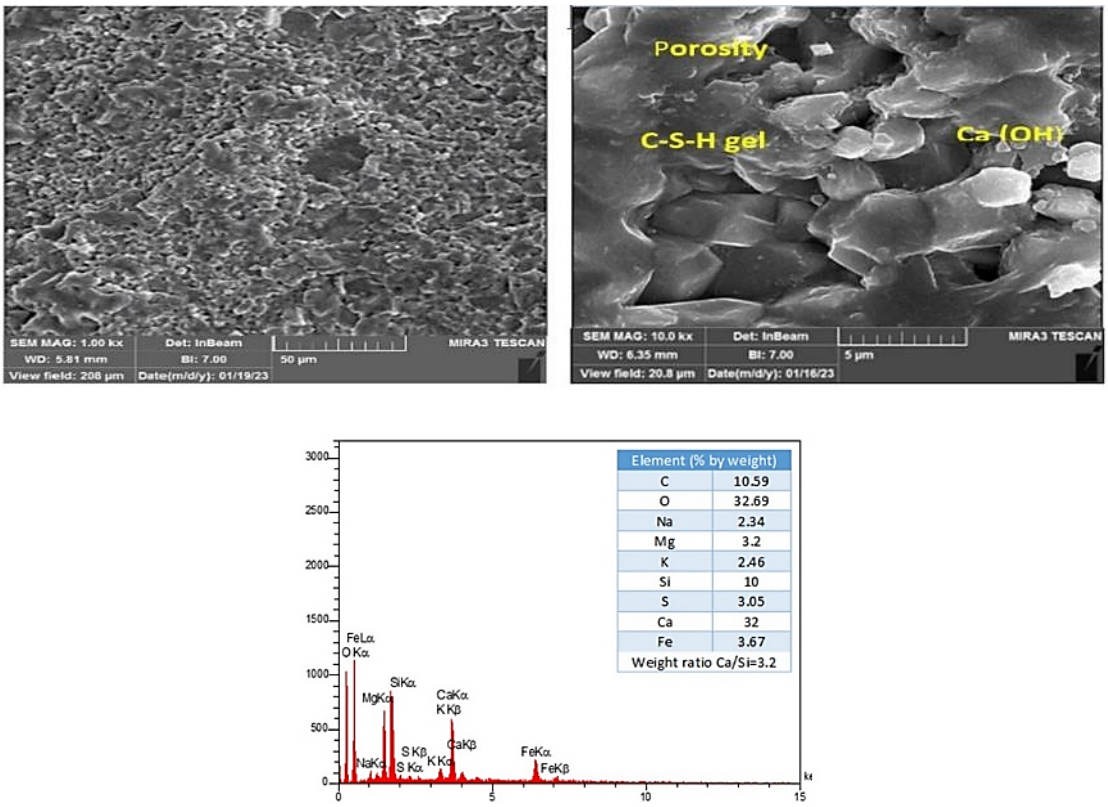

A

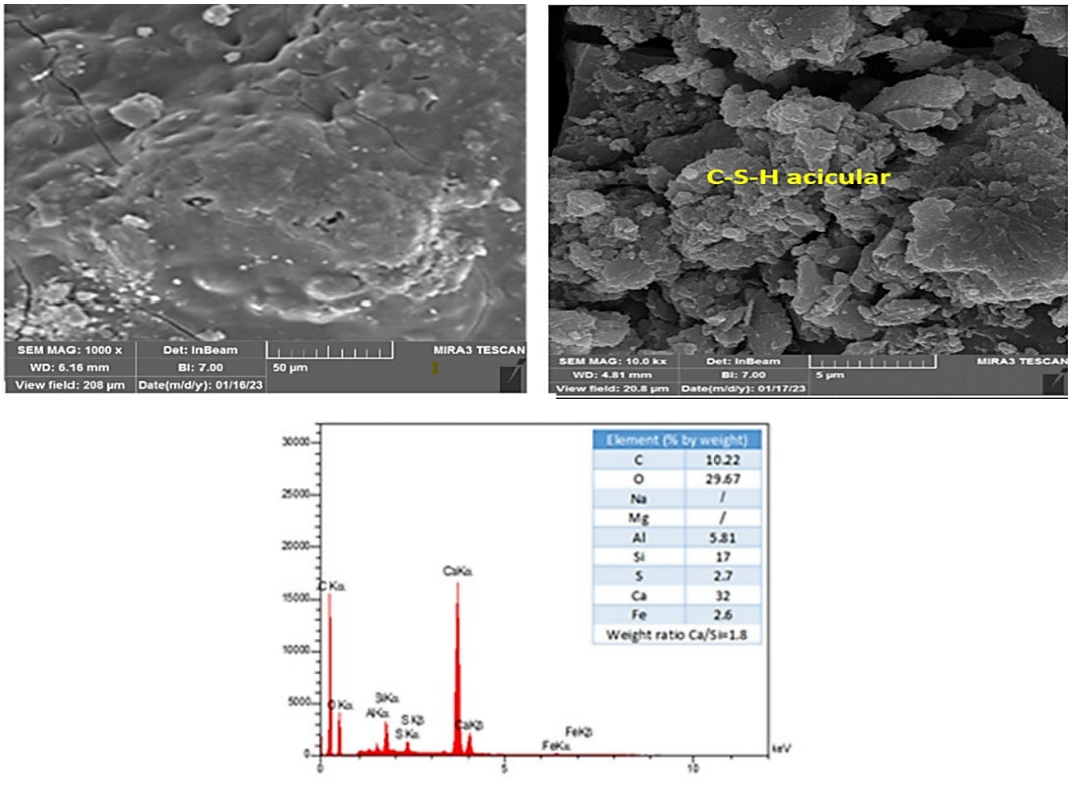

B

Figure 6: Visualizes the pre- and post-self-healing images of cementitious materials captured using (SEM-EDS), (a) the SEM-EDS image of cementitious materials at the 7 day, before they undergo self-healing, (b) the SEM-EDS image illustrates the cementitious materials following healing period, (c) cementitious materials before they self-heal, as seen in the SEM-EDS image taken at 28 days from curing, (d) after 28 days of healing period, the cementitious materials are seen in the SEM-EDS photo

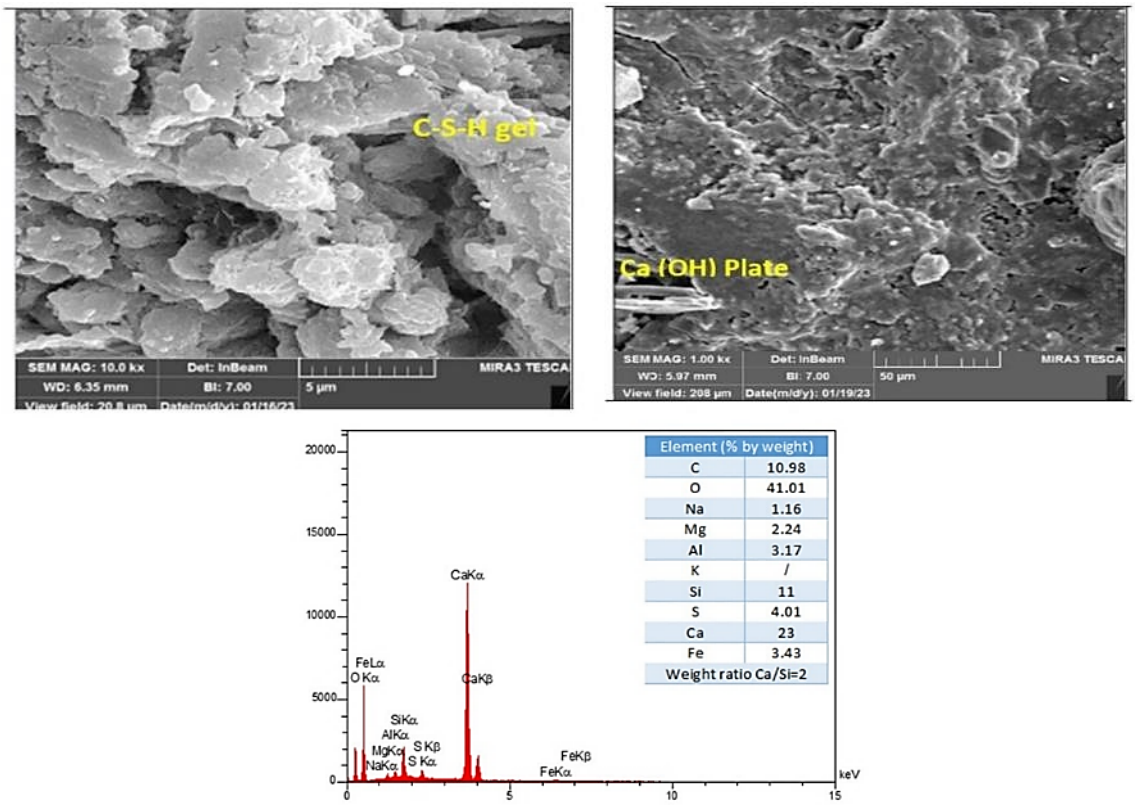

C

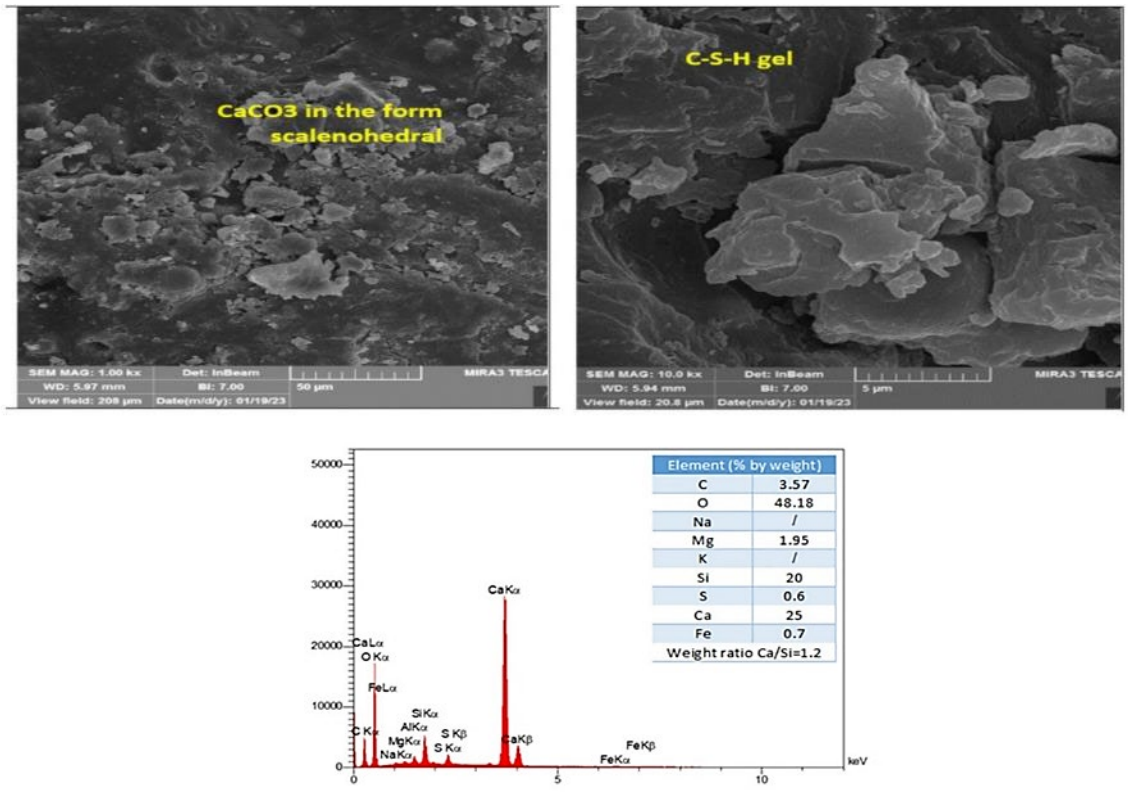

D

Figure 6: Continued

4.5 FTIR

Wide adsorption bands between 3504 and 3417 cm^{-1}, which may be related to O–H, and a band at 874 cm^{-1}, connected to C-H stretching vibration, are among the spectrum characteristics seen in Figure 7. The latter results from the (-CH_2, -CH_3) moiety's deformation vibration. Furthermore, the carbonate bands exhibit discrete maxima between 1423 and 873 cm^{-1}. These peaks represent the C=O angular deformation and antisymmetric stretching, respectively, of calcite ($CaCO_3$).

The FTIR spectra of concrete treated with polycarboxylate superplasticizer, which includes NFA, are shown in Figure 7. The spectrum shows that the surface has many active functional groups. For instance, the transmittance peak of O-H and the stretching vibration peak of C=O may be responsible for the peaks detected at 3477 cm^{-1} and (1425 cm^{-1}, 1576 cm^{-1}), respectively. Furthermore, the diffraction peaks seen at 1111 cm^{-1} at resonance frequencies of the C-O-C vibrations. Reactive functional groupings must be expected for NFA and SP to work together. After the healing period, the SP composite specimen had higher peaks. These specimens' internal molecule-to-molecule interactions and the creation of chemical bonds between molecules might be the sources of this phenomenon. In the Fourier transform infrared (FTIR) analysis of building materials, the peak seen at a wavelength of 2877 cm^{-1} is caused by the existence of the –CH_3 bond group. Furthermore, the size of the C-O-C peaks at 1425 cm^{-1} and 1111 cm^{-1} has increased. There was a distinct peak in the SPFA composite of the specimen. The presence of cross-linking and the detection of chemical bonding in these samples might be the root causes of this phenomenon. A signal with a wavelength of 2877 cm^{-1} is discovered in an FTIR analysis of concrete, indicating the possible existence of the –CH_3 group of functional compounds. Hydrogen bonds are the primary forces between molecules in concrete that facilitate interactions between functional groups of molecules. The user's text is incomplete [48].

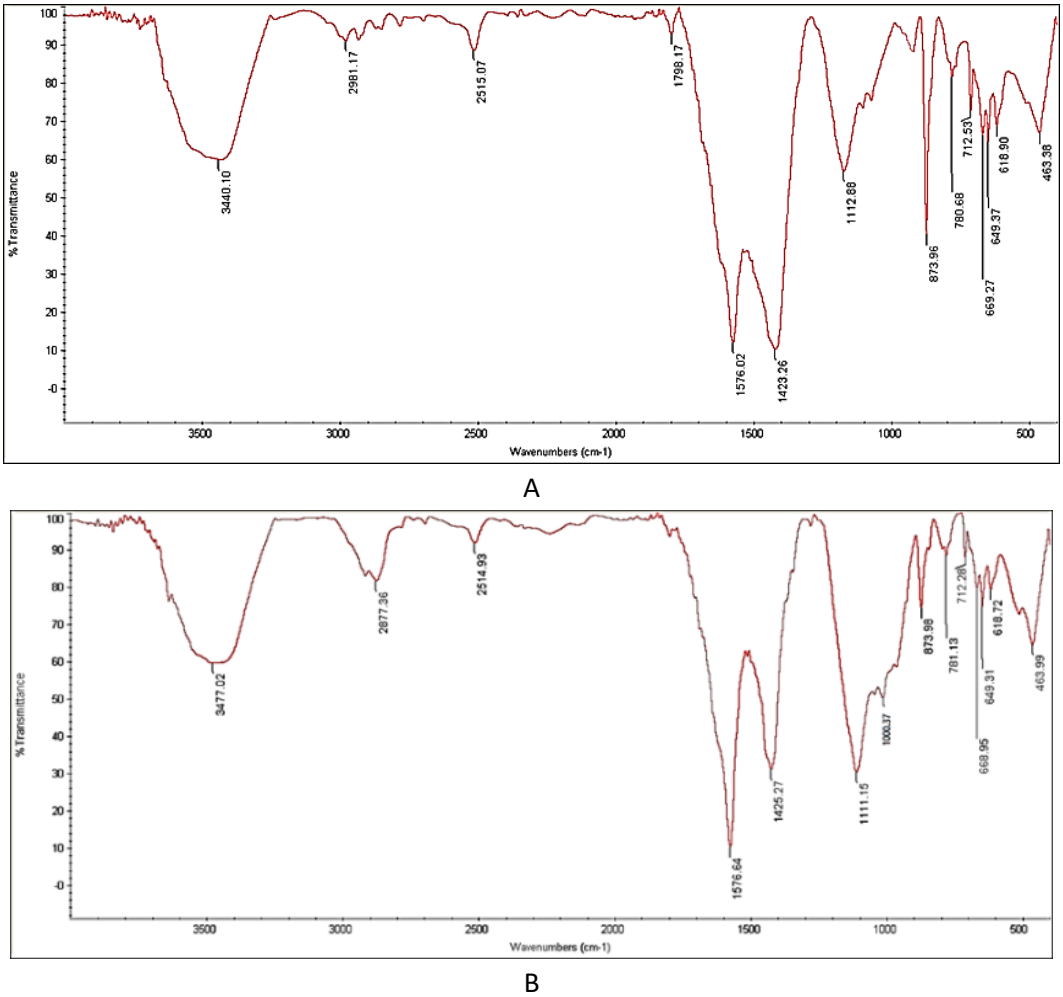

Figure 7: FTIR spectra of (a) the control sample and (b) the sample after the healing period

5. Conclusion

1) The network's reusability is its increased ability to support healing on several levels.
2) The effective injection of powders via a vascular system enhanced the characteristics and sealed the fissures in the concrete beam.
3) The healing process was confirmed when a mechanical repair was found during the second loading cycle.
4) A greater surface area was healed due to the healing agent being injected at many points on the fracture's surface, which enabled the 3D vascular system to cover a greater portion of the crack. In contrast, the (1D) and (2D) systems had lower success rates in obstructing the fracture.

5) Concrete beams' density and compressive resistance increased when the nanopowder was used in conjunction with liquid polycarboxylate ether as a healing agent. As a result, pozzolan interacted better, and the concrete's durability increased. Scanning electron microscopy-energy dispersive X-ray spectroscopy (SEM-EDS) pictures of cementitious materials before and after self-healing show that the NFA decreased permeability by closing the holes and cracks.

Author contributions

Conceptualization, N. Hameed , A. Abdul-Hamead, and F. Othman; methodology, A. Abdul-Hamead. and F. Othman.; validation, F. Othman.; data curation, A. Abdul-Hamead.; writing—original draft preparation, F. Othman; writing—review and editing, N. Hameed , A. Abdul-Hamead, and F. Othman.; supervision, A. Abdul-Hamead, and F. Othman.; All authors have read and agreed to the published version of the manuscript.

Funding

This research received no specific grant from any funding agency in the public, commercial, or not-for-profit sectors.

Data availability statement

The data that support the findings of this study are available on request from the corresponding author.

Conflicts of interest

The authors declare that there is no conflict of interest.

References

[1] A. Formia, S. Terranova, P. Antonaci, N.M. Pugno, J.M. Tulliani, Setup of extruded cementitious hollow tubes as containing/releasing devices in self-healing systems, Materials, 8 (2015) 1897-1923. https://doi.org/10.3390/ma8041897

[2] J. Ahmad, DD. Burduhos-Nergis, M.M. Arbili, S.M. Alogla, A. Majdi, A.F. Deifalla, A review on failure modes and cracking behaviors of polypropylene fibers reinforced concrete, Buildings, 12 (2022) 1951. https://doi.org/10.3390/buildings12111951

[3] B. Šavija, H. Zhang, E. Schlangen, Influence of microencapsulated phase change material (PCM) addition on (micro) mechanical properties of cement paste, Materials, 10 (2017) 863. https://doi.org/10.3390/ma10080863

[4] G.L. Golewski, The phenomenon of cracking in cement concretes and reinforced concrete structures: the mechanism of cracks formation, causes of their initiation, types and places of occurrence, and methods of detection-a review, Buildings, 13 (2023) 765. https://doi.org/10.3390/buildings13030765

[5] A.Z. Dahesh, F.M. Othman, A.A. Abdul-Hamead, Improve Mass Concrete by Controlling the Crack Sealing Mechanism Using Microcapsules of Zinc Oxide, Mater. Sci. Forum, 1002 (2020) 541-550. http://dx.doi.org/10.4028/www.scientific.net/MSF.1002.541

[6] G.F. Huseien, K.W. Shah, A.R.M. Sam, Sustainability of nanomaterials based self-healing concrete: An all-inclusive insight, J. Build. Eng., 23 (2019) 155-171. https://doi.org/10.1016/j.jobe.2019.01.032

[7] B. Šavija, Smart crack control in concrete through use of phase change materials (PCMs): a review, Materials 11(5) (2018) 654. https://doi.org/10.3390/ma11050654

[8] J. Zhu, C. Wang, Y. Yang, Y. Wang, Hygro-thermal–mechanical coupling analysis for early shrinkage of cast in situ concrete slabs of composite beams: Theory and experiment, Constr. Build. Mater., 372 (2023) 130774. https://doi.org/10.1016/j.conbuildmat.2023.130774

[9] M. Roig-Flores, P. Serna, Concrete early-age crack closing by autogenous healing, Sustainability, 12 (2020) 4476. https://doi.org/10.3390/su12114476

[10] Z. Wan, Y. Xu, Y. Zhang, S. He, B. Šavija, Mechanical properties and healing efficiency of 3D-printed ABS vascular based self-healing cementitious composite: Experiments and modelling, Eng. Fract. Mech., 267 (2022) 108471. https://doi.org/10.1016/j.engfracmech.2022.108471

[11] M.M. Meraz, N.J. Mim, M.T. Mehedi, B. Bhattacharya, M.R. Aftab, M.M. Billah, M.M. Meraz, Self-healing concrete: Fabrication, advancement, and effectiveness for long-term integrity of concrete infrastructures, Alex. Eng. J., 73 (2023) 665-694. https://doi.org/10.1016/j.aej.2023.05.008

[12] S.E. Chidiac, M.A. Reda, Performance Modeling of Spherical Capsules during Mixing of Self-Consolidating Concrete, Materials, 16 (2023) 2379. https://doi.org/10.3390/ma16062379

[13] T. Selvarajoo, Characterisation of a vascular self-healing cementitious material system, School of Engineering, Cardiff University, 2020.

[14] M. Siahkouhi, X. Han, M. Wang, A. Manalo, G. Jing, Development and performance evaluation of self-healing concrete railway sleepers using different size PU tubes, Eng. Struct., 283 (2023) 115920.https://doi.org/10.1016/j.engstruct.2023.115920

[15] T. Selvarajoo, R. Davies, D. Gardner, B. Freeman, A. Jefferson, Characterisation of a vascular self-healing cementitious material system: Flow and curing properties, Constr. Build. Mater., 245 (2020) 118332. https://doi.org/10.1016/j.conbuildmat.2020.118332

[16] Z. Wan, Y. Zhang, Y. Xu, B. Šavija, Self-healing cementitious composites with a hollow vascular network created using 3D-printed sacrificial templates, Eng. Struct., 289 (2023) 116282.https://doi.org/10.1016/j.engstruct.2023.116282

[17] Z. Li, L.R. de Souza, C. Litina, A.E. Markaki, A. Al-Tabbaa, A novel biomimetic design of a 3D vascular structure for self-healing in cementitious materials using Murray's law, Mater. Des., 190 (2020) 108572. https://doi.org/10.1016/j.matdes.2020.108572

[18] E. Tsangouri, C. Van Loo, Y. Shields, N. De Belie, K. Van Tittelboom, D.G. Aggelis, Reservoir-vascular tubes network for self-healing concrete: performance analysis by acoustic emission, digital image correlation and ultrasound velocity, Appl. Sci., 12 (2022) 4821. https://doi.org/10.3390/app12104821

[19] J. Feng, H. Dong, R. Wang, Y. Su, A novel capsule by poly (ethylene glycol) granulation for self-healing concrete, Cem. Concr. Res., 133 (2020) 106053. https://doi.org/10.1016/j.cemconres.2020.106053

[20] A. Tonjam, M.M. Mathew, Comparative Performance of Few Self-Curing Agents on Workability and Strength of Self-Curing Concrete, Int. J. Mech. Eng., 7 (2022) 4789-4796.

[21] J. Feng, X.Y. Yap, J. Gao, C.L. Gan, R. Wang, S. Qian, Rapid self-sealing of macro cracks of cementitious composites by in-situ alginate crosslinking, Cem. Concr. Res., 165 (2023) 107074. https://doi.org/10.1016/j.cemconres.2022.107074

[22] A. Torkan, S.M. Hejazi, S.M. Abtahi, M. Shayannejad, Design and fabrication of fibrous media to facilitate autogenous smart self-healing properties in cracked-cementitious structures using polyethylene glycol (PEG) and silicon dioxide nanoparticles, Constr. Build. Mater., 407 (2023) 133518. https://doi.org/10.1016/j.conbuildmat.2023.133518

[23] M. Wu, X. Hu, Q. Zhang, Y. Zhao, Y. Feng, H. Yuan, Synergistic effect of OH-rich fibers and mineral capsules on the self-healing properties of cement mortar, Cem. Concr. Compos., 137 (2023) 104913. https://doi.org/10.1016/j.cemconcomp.2022.104913

[24] S. Sha, M. Wang, C. Shi, Y. Xiao, Influence of the structures of polycarboxylate superplasticizer on its performance in cement-based materials-A review, Constr. Build. Mater., 233 (2020) 117257. https://doi.org/10.1016/j.conbuildmat.2019.117257

[25] G. Anglani, P. Antonaci, S.I.C. Gonzales, G. Paganelli, J.-M. Tulliani, 3D printed capsules for self-healing concrete applications, 10th International Conference on Fracture Mechanics of Concrete and Concrete Structures (FraMCoS-X), Bayonne, France, 2019, 1-12. https://doi.org/10.21012/FC10.235356

[26] S. Iraqi Specifications, IQS 5/1984, for Portland cement, Central Organization for Standardization and Quality Control Baghdad, 1984.

[27] S. ASTM International, ASTM C150-04, Standard Specification for Portland Cement, American Society for Testing and Materials, West Conshohocken, PA, USA, 2004.

[28] S. ASTM International, ASTM C33-03, Standard Specification for Concrete Aggregates, American Society for Testing and Materials, West Conshohocken, PA, USA, 2003.

[29] S. Iraqi Specifications, IQS 5/1984, for Portland cement, Central Organization for Standardization and Quality Control Baghdad, 1984.

[30] S. ASTM International, ASTM C618-22, Standard Specification for Coal Fly Ash and Raw or Calcined Natural Pozzolan for Use in Concrete, ASTM, West Conshohocken, PA, USA, 2022.

[31] S. British, BS 5328-2:1997 Concrete. Methods for specifying concrete mixes (AMD 9691) (AMD 10365) (AMD Corrigendum 10612) (AMD 13877) (Withdrawn), British Standard Institution, London, 1997.

[32] S. British, BS 1881-116:1983, Testing concrete - Method for determination of compressive strength of concrete cubes, British Standard Institution London, 1983.

[33] S. ASTM International, ASTM C78/C78M-16, Standard Test Method for Flexural Strength of Concrete (Using Simple Beam with Third-Point Loading), ASTM, West Conshohocken, PA, USA, 2016.

[34] S. British, BS 1881-116:1983, Testing concrete - Method for determination of compressive strength of concrete cubes, British Standard Institution London, 1983.

[35] S. ASTM International, ASTM C78/C78M-16, Standard Test Method For Flexural Strength Of Concrete (Using Simple Beam With Third-Point Loading), ASTM, West Conshohocken, PA, USA, 2016.

[36] P. Minnebo, G. Thierens, G. De Valck, K. Van Tittelboom, N. De Belie, D. Van Hemelrijck, E. Tsangouri, A novel design of autonomously healed concrete: Towards a vascular healing network, Materials, 10 (2017) 49. https://doi.org/10.3390/ma10010049

[37] S. ASTM International, ASTM E1252-98, Standard Practice for General Techniques for Obtaining Infrared Spectra for Qualitative Analysis, ASTM, West Conshohocken, PA, USA, 1998.

[38] A.I. Thari, S.A. Salih, S.S. Hasan, Influence of using different percentages of waste materials on the strength properties of polymer concrete, IOP Conference Series: Mater. Sci. Eng., IOP Publishing Ltd, 2020, 012067. https://doi.org/10.1088/1757-899X/737/1/012067

[39] S.I. Ibrahim, M. Ramaid, A.H. Ali, The effects of adding nano ZRO_2 on the physical and some mechanical properties of cement paste, J. Eng. Sustainable Dev., 24 (2020) 20-25.http://dx.doi.org/10.31272/jeasd.24.4.3

[40] Z. Al-Moselly, M. Fall, S. Haruna, Further insight into the strength development of cemented paste backfill materials containing polycarboxylate ether-based superplasticizer, J. Build. Eng., 47 (2022) 103859. https://doi.org/10.1016/j.jobe.2021.103859

[41] Z. Li, L.R.d. Souza, C. Litina, A.E. Markaki, A. Al-Tabbaa, Feasibility of using 3D printed polyvinyl alcohol (PVA) for creating self-healing vascular tunnels in cement system, Materials, 12 (2019) 3872. https://doi.org/10.3390/ma12233872

[42] N.A.n. Hameed, F.M. Othman, A.A. Abdul-Hamead, Integration of FDM and self-healing technology: evaluation of crack sealing by durability and mechanical strength, Mater. Res. Express, 10 (2023) 125701. http://dx.doi.org/10.1088/2053-1591/ad0c7d

[43] J. Chen, Y. Zhu, W. Du, M. Li, Y. Wang, C. Zhang, M. Shi, B. Xue, Influence of Polycarboxylate Superplasticizer on the Properties of Cement-Fly Ash Cementitious Materials and Concrete, Sustainability, 14 (2022) 13440. https://doi.org/10.3390/su142013440

[44] C.B. Cheah, W.K. Chow, C.W. Oo, KH Leow, The influence of type and combination of polycarboxylate ether superplasticizer on the mechanical properties and microstructure of slag-silica fume ternary blended self-consolidating concrete, J. Build. Eng., 31 (2020) 101412.https://doi.org/10.1016/j.jobe.2020.101412

[45] P.J. Monteiro, G. Geng, D. Marchon, J. Li, P. Alapati, K.E. Kurtis, M.J.A. Qomi, Advances in characterizing and understanding the microstructure of cementitious materials, Cem. Concr. Res., 124 (2019) 105806. https://doi.org/10.1016/j.cemconres.2019.105806

[46] W. Kunther, S. Ferreiro, J. Skibsted, Influence of the Ca/Si ratio on the compressive strength of cementitious calcium–silicate–hydrate binders, J. Mater. Chem. A., 5 (2017) 17401-17412. https://doi.org/10.1039/C7TA06104H

[47] S. Yang, H. Lee, Drying shrinkage and rapid chloride penetration resistance of recycled aggregate concretes using cement paste dissociation agent, Materials, 14 (2021) 1478. https://doi.org/10.3390/ma14061478

[48] D. Liao, D. Li, S. Zhou, X. Zhang, Y. Fang, Study on the Hydration and Physical Properties of Cement by M18 Polycarboxylate Superplasticizer Modified Graphene Oxide, J. Renew. Mater., 11 (2023) 625-641. http://dx.doi.org/10.32604/jrm.2022.022501